Supporting Online Material for

Anatomy and Dynamics of a Supramolecular Membrane Protein Cluster

Jochen J. Sieber, Katrin I. Willig, Carsten Kutzner, Claas Gerding-Reimers, Benjamin Harke, Gerald Donnert, Burkhard Rammner, Christian Eggeling, Stefan W. Hell, Helmut Grubmüller, Thorsten Lang*

*To whom correspondence should be addressed. E-mail: tlang@gwdg.de

Published 24 August 2007, *Science* **317**, 1072 (2007)
DOI: 10.1126/science.1141727

This PDF file includes:

Supporting Online Material

Materials and Methods

Antibodies

For detection of syntaxin 1 the monoclonal antibody HPC-1 (*S1*) was used. As secondary antibody on immunoblots we applied stabilized goat anti-mouse HRP-conjugated antibodies (product No. 1858413, Pierce). For immunofluorescence sheep-anti-mouse immunoglobulins G (catalogue No. 515-005-003, Dianova) were labeled with the fluorescent dye Atto532 or Atto647N (provided by K. H. Drexhage, Dept. of Chemistry, University of Siegen, Germany).

Plasmids

Plasmids for transient overexpression of rat syntaxin 1A (Sx1A)/syntaxin 1A-constructs under the control of the CMV promoter were produced by standard molecular biological methods. The encoded proteins were tagged with monomeric green fluorescent protein (mGFP), a variant of enhanced green fluorescent protein carrying the single amino acid substitution A206K, which has been shown to prevent dimerization of fluorescent proteins (*S2*).
All constructs are derived from pEGFP-N1 (Clontech, Mountain View, CA) (GenBank accession No. U55762) and encode fusion proteins, in which 12 amino acids (LVPRARDPPVAT) connect the protein of interest to the mGFP-tag (with the exception of open Sx1A-GFP (*S3*): the linking sequence was here PPVAT).
The plasmids used for transient overexpressions coded for the following fusion proteins: Sx1A-GFP [Sx1A-(1-288) + mGFP] (*S4*); Sx1AmutTMR-GFP [Sx1A-(1–288 carrying the mutations M267A, C271A, and I279A) + mGFP] (*S4*); open Sx1A-GFP [Sx1A-(1–288 carrying the mutations L165A and E166A) + mGFP] (*S3*); Sx1A, SNARE motif-TMR-GFP [Sx1A-(1–28 + 183–288) + mGFP] (*S4*); Sx1A, TMR-GFP [Sx1A-(1–28 + 259–288) + mGFP] (*S4*); -5Δ [Sx1A-(1-28 + 206-217 + 259-288) + mGFP]; -5 [Sx1A-(1–28 + 206–288) + mGFP]; -4 [Sx1A-(1–28 + 210–288) + mGFP]; -3 [Sx1A-(1–28 + 213–288) + mGFP]; -2 [Sx1A-(1–28 + 217–288) + mGFP]. Coding sequences of all constructs have been verified by sequencing using the according rat sequences as references.

Cell culture and transfection

PC12 cells (clone 251) (*S5*) were maintained, propagated and transfected essentially as described (*S6*), except that for transfection 20–30 µg of plasmid DNA were used per cuvette. Experiments were carried out approximately 20-60 h post-transfection.

Membrane sheets preparation

Membrane sheets were prepared as previously described (*S4*, *S7*). In brief, cells were grown on poly-L-lysine-coated coverslips and disrupted by ultrasound treatment in ice cold sonication buffer (120 mM potassium glutamate, 20 mM potassium acetate, and 2 or 10 mM EGTA, 20 mM HEPES pH 7.2).

Immunofluorescence

In order to exclude crosslinking of syntaxin molecules by antibody treatment (*S6*), freshly prepared membrane sheets derived from PC12 cells were immediately fixed for 90–120 min at room temperature in 4% paraformaldehyde in phosphate-buffered

saline (PBS) (137 mM NaCl, 2.7 mM KCl, and 8.1 mM Na_2HPO_4, pH 7.3) and immunostained using standard protocols, essentially as described (*S6*). Stimulated emission depletion (STED) microscopy was carried out on HPC-1/sheep-anti-mouse-Atto532 and HPC-1/sheep-anti-mouse-Atto647N stained coverslips mounted in Mowiol [6 g Glycerol AR (No. 4094, Merck, Darmstadt, Germany), 2.4 g Mowiol 4-88 (Hoechst, Frankfurt, Germany), 6 ml water, 12 ml 200 mM Tris, pH 7.2]. Prior to mounting, the Atto647N samples were post-fixed for at least 15 min with 10% PFA and washed three times with PBS.

Analyzing syntaxin 1 cluster density

The average number of syntaxin clusters per μm^2 was determined by image analysis on STED micrographs of immunostained membrane sheets as shown in Fig. 1A (using HPC-1/sheep-anti-mouse-Atto532 as antibodies) in principle as described (*S4*), except that images were filtered using only the blur (10%) option in Metamorph 4.1.7 (Universal Imaging Corporation) and that 2.25 μm^2 regions with fixed manual scaling to enhance spotty structures were printed for analysis (only clusters but not individual molecules are counted using this methods). We applied a similar STED microscope setup (with an effective focus of 72 nm) as previously described (*S4*).

Determination of cluster size

To determine cluster size we imaged membrane sheets immunostained for syntaxin 1 applying a different STED microscope as for the analysis of cluster density. For Fig. 1B, we used a secondary antibody labeled with the dye Atto 647N (Atto-Tec, Germany), emitting at ~ 670 nm. The dye was excited with a pulsed laser diode at 635 nm (~ 70 ps pulse width, Picoquant, Germany) and fluorescence detected between 660 – 700 nm (using an avalanche-photodiode). We used a Ti:Sa laser (Mira, Coherent) to supply the pulsed (~ 200 ps pulse width) STED light at 750 nm with a repetition rate of 76 MHz. We also used the 76 MHz repetition rate of the STED laser to trigger the excitation laser diode. The average excitation and STED power at the focal plane was 12 µW and 73 mW, respectively.

We determined the FWHM (full width at half maximum) of each single cluster by a Lorentzian fit to their spatial intensity distribution as in detail outlined in (*S8*). The diameter of the effective focus (point spread function (PSF)) of the STED microscope was 53 nm as established by images of Atto 647N labeled antibodies (Fig. S1). The effective PSF as well as the theoretical distribution of labeled antibodies within the clusters were included for the final estimation of the cluster diameter. Hence, the measured FWHM of approximately 68 nm of the imaged cluster suggest an average cluster size of 50-60 nm. Especially due to the variation in potential distribution of labeled antibodies within the clusters, the cluster size estimate statistical error is ± 5 nm.

Determination of the cell surface

PC12 cells were detached from their substrate as previously described (*S6*) and the cell pellet was resuspended in PBS (137 mM NaCl, 2.7 mM KCl, and 8.1 mM Na_2HPO_4, pH 7.3). Under these conditions the PC12 cells adopt a spherical shape that is maintained for a couple of minutes after the cell adsorbed to a glass cover-slip. Optical sectioning of these spherical cells was performed applying a confocal microscope. The equatorial plane was used to determine the cell diameter by linescan analysis (compare Fig. S2). In total 85 cells were analysed from four independent preparations. From the PC12 diameter of 12.1 µm (Fig. S2) we calculated that the cell

surface covers an area of approximately 460 μm^2. This is a lower limit as membrane ruffles seen occasionally in electron micrographs of similar preparations are not detected by the analysis.

Fluorescence recovery after photobleaching (FRAP) experiments and confocal imaging with intact cells

PC12 cells grown on poly-L-lysine coated coverslips were mounted in Ringer solution (130 mM NaCl, 4 mM KCl, 1 mM $CaCl_2$, 1 mM $MgCl_2$, 48mM D(+)glucose, 10 mM HEPES pH 7.4) and the basal plasma membrane was imaged at RT using a 100x 1.4 numerical aperture plan apochromat oil objective of an inverted confocal laser scanning microscope (TCS-SP2; Leica Microsystems, Mannheim). GFP fluorescence was excited using the 488 nm line of the Ar ion laser and emission was collected between 500 and 600 nm at a 1 Airy disc pinhole size. Pixel size was 147 nm x 147 nm. Scanning was performed at 400 Hz with laser power set to 3.5 % (gain 700V; offset 0.5-0.7%). Bleaching was carried out with laser power set to 100 %. FRAP experiments were performed using the FRAP-wizard of the Leica Confocal Software Version 2.5 Build 1347 (Leica Microsystems, Mannheim). 10 frames were recorded at maximal speed (1.02 s/frame) before a region of 2.93 µm x 2.93 µm was bleached twice (using the 'zoom in' option), then 10 frames were recorded at maximal speed followed by 48 frames at a rate of 12 frames per minute. At the end of the experiment again 10 frames were recorded at maximal speed. For brightfield imaging gain and offset were adjusted to 480V and 0%, respectively. The obtained data were analyzed using MS-Excel 2000 and Origin (Microcal Software, Inc., Northampton, MA). The background corrected fluorescence signal obtained for the region of interest (ROI) was normalized to the pre-bleach value (average of the 10 frames recorded before the bleaching steps) for each time point (t) of a given recording. This procedure allowed averaging of traces obtained for individual cells measured the same day (compare Fig. S6, for one independent experiment 4-10 cells were averaged per day and construct). The following equation was used for signal normalization:

$$signal_{ROI\ normalized}(t) = \frac{signal_{ROI}(t)}{signal_{ROI}(pre\ bleach)}$$

The obtained averaged traces (with time set to 0 for the first frame post bleach) were fitted as described (*S9*) applying an hyperbola function with off set:

$$signal_{ROI\ normalized}(t) = a + b \times t/(t_{1/2} + t),$$

where $t_{1/2}$ corresponds to the half-maximum recovery time, a is the offset of the curve and b is the amplitude of the recovery curve. Note that, as the laser power should have been strong enough to achieve complete bleaching, the observed off set is most likely caused by slow scanning and therefore more prominent for faster constructs. We did not observe a correlation between expression level of syntaxin 1A-GFP and recovery time (compare Fig. S7) indicating that under our experimental conditions the ratio between endogenous and overexpressed syntaxin did not have any influence on recovery. Experiments exhibiting a z drift of the focal plane, identified by the intensity variation of an unbleached control region of the basal plasma membrane, were excluded from the analysis.

Apparent lateral diffusion coefficients were determined from the half times of recovery according to Ficz et al. (*S9*) using correction factors for the ROI geometry (*S9, S10*) yielding 0.014 $\mu m^2/s$ for full-length syntaxin 1A and 0.055 $\mu m^2/s$ for the TMR-only construct of syntaxin. Kinetic fitting for fast diffusing molecules requires extrapolation of the first (fast) phase that cannot be recorded (see above) resulting in a systematic overestimation of the diffusion coefficient. To be on the safe side, we have avoided extrapolation for the data shown in Fig. 2 (therefore differences in mobility represent lower limits) whereas for the modelling we used for the TMR-only construct a value of 0.075 $\mu m^2/s$ ranging between the over- and the underestimated value. However, some caution needs to be exerted when comparing diffusion coefficients determined in different studies as no accepted standards are available for fitting and for other experimental parameters such as temperature.

FRAP experiments on membrane sheets

Membrane sheets derived from transfected PC12 cells were prepared as described above, mounted in sonication buffer at RT and FRAP experiments were performed as described for intact cells. In contrast to intact cells, for membrane sheets the total fluorescence of the preparation is known and allows correcting the obtained signal for e.g. bleaching, laser fluctuation etc. before normalization. The obtained netto signal at each time point (t) of a given recording was corrected and normalized using the following equation:

$$signal_{corrected\ and\ normalized}(t) = \frac{signal_{whole\ membrane\ sheet}(pre\ bleach)}{signal_{whole\ membrane\ sheet}(t)} \times \frac{signal_{ROI}(t)}{signal_{ROI}(pre\ bleach)}$$

Correction becomes necessary as in this type of experiments a much larger relative proportion of the total fluorescence is lost during the bleaching step, compared to the ones performed with intact cells, in which the bleached ROI represents only approximately 1/50 - 1/60 of the total cell surface. This correction does not affect half times and allows exact determination of maximal recovery, in contrast to experiments using intact cells, in which incomplete recovery could in theory represent equilibrium between recovery and bleach during acquisition. The data obtained from 8-10 membrane sheets were averaged for each independent experiment.

Epi-fluorescence microscopy and correlation analysis

Membrane sheets from cells expressing Sx1A-GFP were prepared and mounted in a microcopy chamber filled with RT sonication buffer. For conventional, diffraction limited fluorescence microscopy a Zeiss Axiovert 100 TV fluorescence microscope with a 100X 1.4 numerical aperture plan apochromat oil objective (Zeiss, Göttingen, Germany) was used. Illumination was provided by a XBO 75 xenon lamp (Zeiss, Göttingen, Germany). For imaging, we applied a back-illuminated charge-coupled device camera (Princeton Instruments, Princeton, NJ) with a magnifying lens (2.5x Optovar; Zeiss, Göttingen, Germany) to avoid spatial undersampling by large pixels. The focal position was controlled using a low voltage piezo translator device and a linear variable transformer displacement sensor/controller (Physik Instrumente, Waldbronn, Germany). Addition of 1-(4- trimethyl-ammoniumphenyl)-6-phenyl-1,3,5-hexatriene (TMA-DPH, Molecular Probes) visualized phospholipid membranes and allowed assessment of membrane integrity. Appropriate filter sets were used for TMA-DPH [excitation bandpass (BP) 360/50, beamsplitter (BS) 400–420, and

emission longpass (LP) 420] and GFP [excitation BP 480/40, BS LP 505, and emission BP 527/30]. Image acquisition was performed with Metamorph 5.1 (Universal Imaging, West Chester, PA). In time-lapse experiments GFP fluorescence was recorded over 5 min at intervals of approximately 15 seconds (1 s exposure time), followed by taking an image in the TMA-DPH channel (1 s exposure time) documenting the integrity of the membrane sheet. During the time course more than one third of the GFP fluorescence was bleached. Images shown in Fig 3 are autoscaled. To quantitate objectively the degree of similarity between the last and the first image of a given time series, we calculated the Pearson correlation coefficient. To this end, a region of interest (ROI) was defined that covered a large area of the membrane sheet, but excluded membrane inversions at the rim. A custom designed, previously described (*S4*) MATLAB 7.0.1.24704 (The MathWorks, Natick, MA) routine was applied to determine the Pearson correlation coefficient of the two images within the ROI. Only membrane sheets with an average netto fluorescence signal of at least 40 counts per pixel for the last GFP image were included in the analysis. 16 membrane sheets from three independent days were analyzed resulting in an average correlation coefficient of 0.82 ± 0.11 (mean ± SD).

Quantitative immunoblot

The concentration of previously harvested PC12 cells was determined using a Neubauer-chamber and cell lysates obtained pelleting a defined number of cells. The cell pellets were incubated for 30 min at 4° C under continuous head-over-head rotation in 1 ml per 5 million cells of lysis buffer [150 mM NaCl, 5 mM EDTA, 1% Triton X-100, 0.5% deoxycholate, complete EDTA-free protease inhibitor cocktail (Roche, Mannheim), 50mM Tris pH 7.4]. Lysates were centrifuged for 8 min (16,000 g; 4° C) and supernatants were used for the experiments. PC12 cell lysates of 10,000 cells and 2.3 – 60 fmol of recombinant syntaxin 1A [amino acids 2-288 of rat syntaxin 1A carrying a N-terminal myc-tag (GSHMKLATM*EQKLISEEDL*NS), kind gift from Dr. Matthew Holt] were immunoblotted. Compared to PC12 cell lysates, samples for calibration contained the same amount of protein (μg) from BHK cell lysate that is devoid of syntaxin 1 (obtained as described above for PC12 cells), in order to mimic the presence of other proteins within the lane of the immunoblot. The monoclonal antibody HPC-1 was used to detect syntaxin 1 (used at a dilution of 1:1000). Blots were washed and then further incubated with HRP-conjugated secondary antibodies (1:500). Detection was performed using enhanced chemiluminescence reagents (SuperSignal West Dura Extended Duration Substrat, catalogue No. 34075 Pierce) and a LAS-1000 reader (Fujifilm). Bands were quantified densiometrically using Metamorph 4.1.7 (Universal Imaging Corporation) and intensity values were corrected for background. The number of syntaxin molecules per cell was then determined from standard curves. In our approach to determine the number of syntaxin molecules per cluster, all syntaxin 1 is assumed to be present at the plasma membrane. The distribution of syntaxin 1A-GFP indicates that syntaxin indeed is almost exclusively plasma membrane associated. However, it cannot be ruled out that a minor fraction is not localized at the plasma membrane. For this reason, and because the cell surface of 460 μm^2 is a lower estimate, the number of syntaxin molecules per cluster represents an upper estimate.

In silico modelling of supramolecular syntaxin

Using the 3D program Maya (Autodesk Inc., San Rafael, CA, USA), we first created the elongated conformation of a perpendicular syntaxin 1A molecule with minimal

area consumption in the lateral plane. To this end we used structural data of the N-terminal domain (PDB coordinate: 1BRO) and the SNARE-motif (PDB coordinate: 1HVV) of syntaxin 1A. The remaining amino acids were added. Then 75 syntaxin molecules were packed with minimal space occupancy of their SNARE-motifs. As a result, the linker regions between the N-terminal domains and the SNARE-motifs were bent to different degrees according to their positions in the resulting structure. For comparison also a second structure was created in which the N-terminal domains were packed at highest density

Brownian dynamics simulations

Lateral diffusion of the syntaxin molecules within the plasma membrane was described by Brownian dynamics simulations (*S11*). Initially, n=1391 syntaxin molecules were placed at random, non-overlapping positions $\mathbf{r}_i=(x_i, y_i)$, $i=1\ldots n$, within an area of $0.879\times0.879\ \mu m^2$, as shown in Fig. 4A (left) in the main text. The number of syntaxin molecules is based on experiments that determined the endogenous syntaxin concentration. In FRAP experiments syntaxin was overexpressed causing a proportional increase in the number of syntaxin clusters (*S4*). However, recovery speed is not dependent on expression levels (see Fig. S7) indicating that not the total amount of syntaxin but the ratio of clustered to free molecules determines recovery characteristics. Therefore we can use the endogenous syntaxin concentration as a value for the simulation.

Brownian diffusion was simulated by recursive update of the syntaxin positions satisfying the diffusion equation, for the probability $p(\mathbf{r}_i,t)$ to find a syntaxin molecule at position $\mathbf{r}_i$ at time t

$$\partial_t\, p(\mathbf{r}_i,t) = \nabla_i D[\nabla_i - \beta \mathbf{F}_i(\mathbf{r}_i)]\, p(\mathbf{r}_i,t) \tag{1.1}$$

with the drift force term $\mathbf{F}(\mathbf{r}_i)=-\nabla_i\, U(\mathbf{r}_1,\ldots\mathbf{r}_n)$ derived from an interaction potential

$$U = \sum_{i<j}^{n} V(r_{ij}) \tag{1.2}$$

composed of pairwise interactions acting between individual syntaxin molecules

$$V(r_{ij}) = E_1 e^{-r^2/2\sigma^2} - E_2 f_s e^{-r^2/[2(2\sigma)^2]}. \tag{1.3}$$

No explicit diffusion traps were used. Here, $r_{ij}=|\mathbf{r}_i-\mathbf{r}_j|$ is the distance between syntaxin molecules i and j, $\beta = 1/k_B T$ is the reciprocal thermal energy at room temperature. The first term of V describes the mutual repulsion of strength E_1 and range σ that prohibits molecules from running through each other (Pauli repulsion); the second term describes an effective attraction of strength E_2 and range 2σ between the syntaxin molecules, mediated by the SNARE-motifs that drive syntaxin clustering. By using an effective potential, possible low-molecular oligomerization was accounted for in a mean field sense. The range σ was chosen such that an approximate area per syntaxin TM helix of 1.5 nm^2 was obtained (*S12*), i.e., such that the minimum of V is at $\sqrt{1.5}$ nm. The strength of the attractive interaction between the syntaxin molecules,

i.e. the depth of the minimum of V (see inset in Fig. 4B), was used as one of the two adjustable parameters.

To describe the assumed sterical hindrance due to the bulky helical syntaxin regions, which increases with cluster size, a scaling factor $f_s=1-(n_c/n_{max})^2$ was included. This factor weakens the effective attraction for increasing cluster size n_c; for $n_c \geq n_{max}$ the interaction thus becomes repulsive, thereby preventing further cluster growth (Fig. 4B inset). The simulations that were in agreement with the experimental cluster density are shown in Fig. 4B and used n_{max} = 140, with the exception of the red trace (n_{max} = 60) and the black trace (n_{max} = 120). For determination of cluster size, a distance criterion was used, i.e., two syntaxin molecules were assigned the same cluster if their mutual distance was below 1.5 nm. The value for n_{max} determines the strength of the repulsive component and was used as the second adjustable parameter.

Trajectories satisfying the diffusion equation were obtained numerically by time discretization. Accordingly, the molecular positions were recursively updated,

$$\mathbf{r}_i(t+\Delta t) = \mathbf{r}_i(t) - D\Delta t\cdot\mathbf{F}_i(t) + \xi\sqrt{2D\Delta t}\,, \qquad (1.4)$$

where ξ is a random number drawn from a (two-dimensional) normal distribution with variance one. Periodic boundary conditions and an integration step size of Δt=30.6 ns were used, which was determined to trade off efficiency and numerical stability.

To improve convergence, the simulation system was scaled down (with unchanged syntaxin number density) by a factor of 10 with respect to the experimental set-up, implying 10^2=100 times faster fluorescence recovery kinetics. In Fig. 4B of the main text, the time axis has been scaled accordingly to facilitate direct comparison with experimental data. For the simulation of the TMR construct, f_s was set to zero, in accordance with the experimental finding that it is not sorted to syntaxin clusters.

Experimental data shown in Fig. 2C were used for Fig 4B and the amplitudes of the fluorescence recovery curves rescaled by $A_t/(A_t-A_b)$, where A_t is the total plasma membrane area and A_b the bleached area. For the simulations, $A_b=A_t/9$, implying a scaling factor of 9/8. Since the diffusion coefficient D (0.075 $\mu m^2/s$, see above) is dominated by the membrane and not by the solvent, this value is used in the simulations for full length syntaxin.

The strength of the attractive part of the interaction potential as well as the strength of the repulsive component were varied until optimal agreement between simulated and measured recovery curves was obtained. As an experimental constraint, only those parameter combinations were considered, where the average number of syntaxin clusters obtained from the simulation agreed with the measured value of 19.6/μm^2. To reduce statistical fluctuations, recovery curves from 36 different bleaching areas in two subsequent runs were averaged for each case.

Traces were corrected for bleaching effects occurring in FRAP experiments. In our FRAP experiments, a small fraction s of fluorescent syntaxin molecules was bleached during each image acquisition. The value of s can be estimated using the decay of the experimental FRAP curves during the last 10 image acquisitions at higher frequency at t approx. 250 s. Assuming that recovery is negligible, s can be computed from the intensity $s = 1-(I_a^{exp}/I_b^{exp})^{1/10}$ yielding s = 0.005. We have included this bleaching effect in the simulated FRAP curves by simulating the 68 data acquisitions of the experiment. Starting at t = 0 seconds, the simulated FRAP curve is left

unaltered until in the experiment an image at time t_i is taken. As a first step, the signal values for $t \geq t_i$ are reduced by the factor s to account for the experimental bleaching. Thus, at t_i the signal I is reduced from $I(t_i)$ to $I(t_i)\cdot(1-s)$. The bleached fraction $s\cdot I(t_i)$ will now also recover since these syntaxin molecules are also in constant exchange with the unbleached molecules outside the bleach area. This fraction is indeed subject to the very recovery kinetics that is given by the (uncorrected) signal curve. Therefore, as a second step, a bleach recovery signal R has been added to the signal curve starting at t_i, with $R(t) = 0$ for $t \leq t_i$ and $R(t) = s\cdot I(t_i)\cdot I(t-t_i)$ for $t > t_i$. Starting at the time of the first acquisition, this procedure was sequentially applied at all acquisition times t_i.

From the simulation we extracted the statistics of dissociation rates of syntaxin monomers from the clusters. Fig. S5 shows these data which has been obtained as follows. For every syntaxin monomer that leaves a cluster (a cluster is defined to contain at least 10 molecules) at a certain instance of time during the simulation, this dissociation event is recorded, together with the residence time τ it has spent within the respective cluster. The obtained histogram $h(\tau)$ of residence times τ was then decomposed into its individual decaying exponentials by applying a Laplace analysis, $c(\tau) = \Sigma_\sigma\, g(\sigma)\sigma^{-1}e^{-\tau/\sigma}$, yielding a distribution $g(\sigma)$ of dissociation time constants σ. For the histogram, a logarithmic binning was used. For the Laplace analysis, weak regularization in terms of minimizing the (integrated) second derivative of $g(\sigma)$ was applied (*S13*).

Supplementary Figures

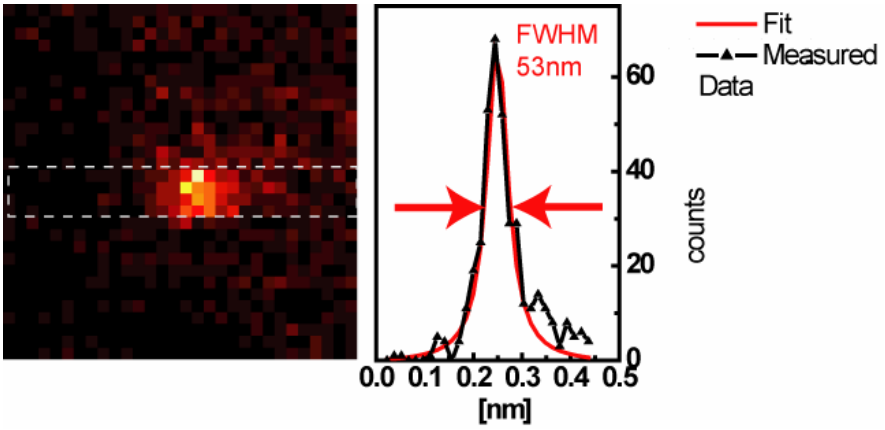

Figure S1. Resolution of the STED microscope
In order to determine the resolution of the experimental set-up, single primary antibodies were imaged under the same labeling conditions (Atto647N labeled secondary antibodies), the same mounting media and with the same excitation and STED power as in the syntaxin cluster measurements. Exemplary image of a single antibody (left) and horizontal line profile (right, summed up over 4 lines) providing a FWHM of 53 nm from a Lorentzian fit to the data. The profiles recorded for 112 single antibodies were summed up and fitted providing a median spot diameter of ~ 53 nm.

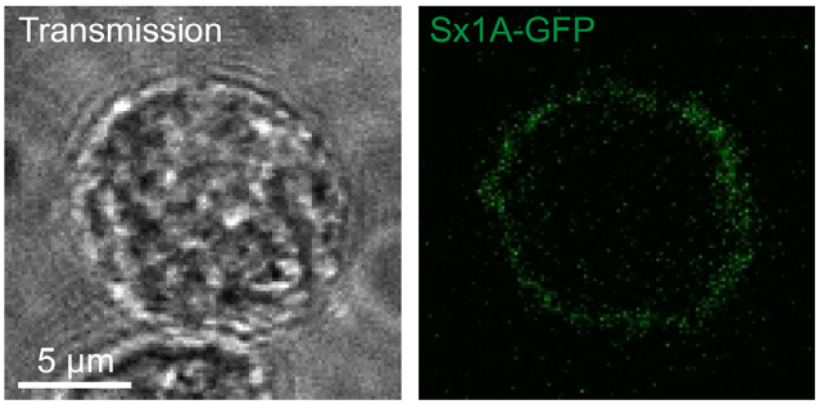

Figure S2. Diameter of PC12 cells
Confocal micrograph of spherical PC12 cells. One of them is expressing Syntaxin 1A-GFP that marks the plasma membrane. The cell diameter was determined from the equatorial plane in the GFP-channel, yielding 12,1 µm ± 1,5 µm (mean ± SD, n= 85 cells). Left, brightfield, right confocal section taken in the GFP-channel.

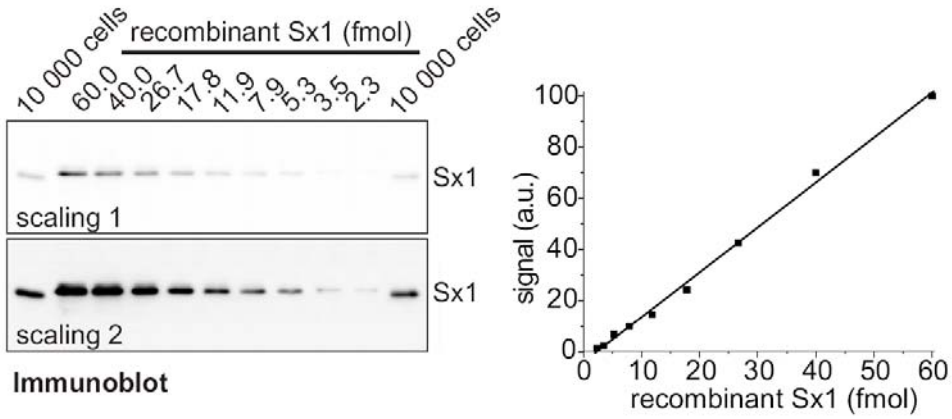

Figure S3. Determination of the number of syntaxin 1 molecules per PC12 cell
Syntaxin 1 bands of immunoblotted PC12 cell lysate and samples for calibration were analysed densitometrically (two different scalings are shown). From the standard curves we determined 830,000 ± 200,000 syntaxin 1 molecules to be present in an average PC12 cell (mean ± SD, n = 6 independent experiments).

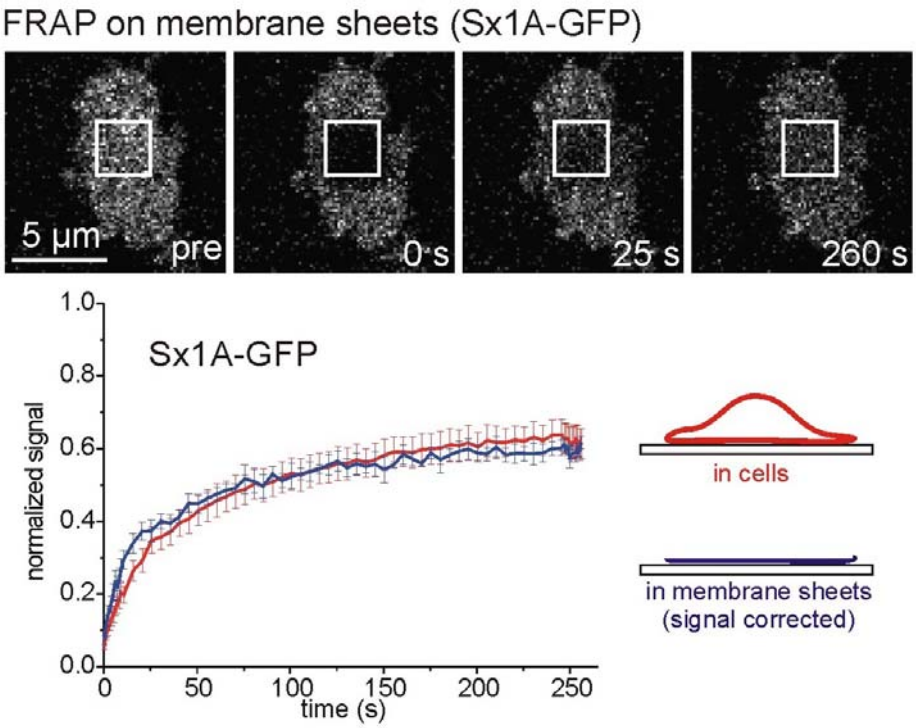

Figure S4. FRAP on membrane sheets
FRAP on membrane sheets (blue trace, n = 3 experiments; for comparability signal has been corrected for bleaching) and intact cells (red trace, n = 9 experiments including experiments from Fig. 2B and C and e.g. experiment shown in Fig. S6). Values are mean ± SEM. Membrane sheets were generated by a brief ultrasound pulse (see methods for details). Generation of membrane sheets results in fast wash-out of cytosolic components including e.g. G-actin and ATP. As an effect, actin reorganization is stopped (with the exception of stress fibers) leading to thinning out of the actin meshwork.

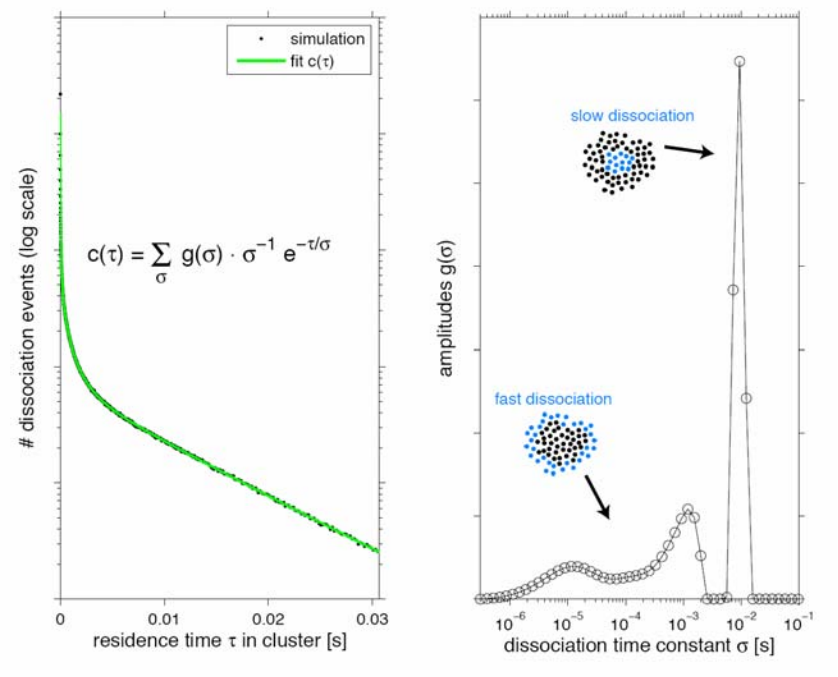

Figure S5. Dissociation statistics and spectrum of dissociation time constants.
Left, histogram h(τ) of dissociation events, extracted from the Brownian dynamics simulation, as a function of cluster residence times τ (black dots). Green line, c(τ) fit to the data with g(σ) that were obtained by an inverse Laplace transform of the residence time histogram (see Methods).
Right, spectrum g(σ) of dissociation time constants σ. The sharp peak to the right corresponds to slow dissociation (escape) of deeply buried syntaxin molecules (blue); the broad distribution of dissociation times to the left side of the spectrum corresponds to fast dissociation of molecules at the cluster rims.
Note that in general, for decompositions of decay curves into more than three or four exponentials, slightly different decompositions typically fit the data equally well. Therefore, care has to be taken not to over-interpret details of the obtained spectra. For the case at hand, both the sharp peak at the right as well as the broad band at the left are reliable features, but not the detailed structure of the band.

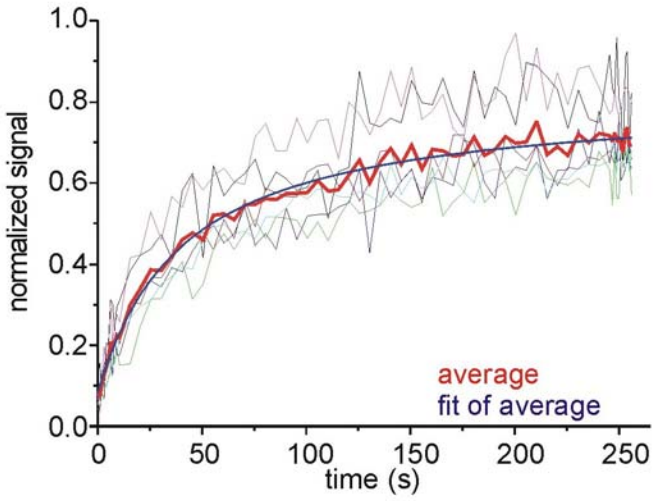

Figure S6. Variation of recovery traces between cells and data processing
Traces from one experiment showing individual cells (differently colored fine lines). Red solid line, average of individual traces. Blue line, fit of average trace from which the half time was determined. For experiments in Fig. 2B and C fitting was performed as shown; for experiments in Fig. 2D and E the last 10 data points recorded at high frequency were omitted.

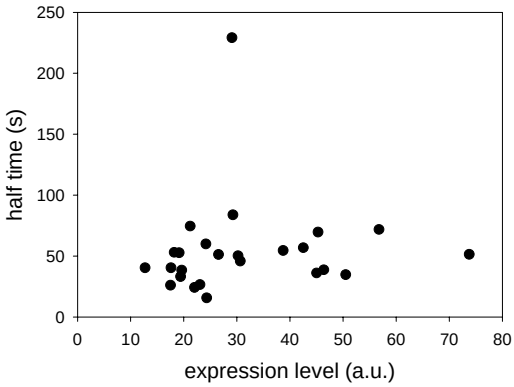

Figure S7. Half time of recovery is independent from expression level
Data from experiment shown in Fig. 2C for Sx1A-GFP. The half time shown in Fig. 2C is the average of three experimental days, and for each day several cells have been analyzed. In this plot, for each of the individual cells half time of recovery is plotted versus expression level (image intensity of the confocal micrographs taken at fixed settings). No correlation between half time of recovery and expression level can be observed, even the one strongly overexpressing cell (image intensity of approximately 75 a.u.) has a normal recovery rate. Only in one case we observed an unusually slow half time of recovery, but this was obviously not related to the expression level. As discussed in our previous paper (*S4*), syntaxin 1 can be overexpressed up to 5-fold over endogenous levels. However, in our experiments we tended to select cells with lower expression levels (see figure). We assume that the average overexpression level was 2-3 fold over endogenous syntaxin.

Supplementary References

S1. C. J. Barnstable, R. Hofstein, K. Akagawa, *Brain Res* **352**, 286 (Jun, 1985).
S2. D. A. Zacharias, J. D. Violin, A. C. Newton, R. Y. Tsien, *Science* **296**, 913 (May 3, 2002).
S3. F. E. Zilly, J. B. Sorensen, R. Jahn, T. Lang, *PLoS Biol* **4**, e330 (Sep 26, 2006).
S4. J. J. Sieber, K. I. Willig, R. Heintzmann, S. W. Hell, T. Lang, *Biophys J* **90**, 2843 (Apr, 2006).
S5. R. Heumann, V. Kachel, H. Thoenen, *Exp Cell Res* **145**, 179 (Apr 15, 1983).
S6. T. Lang *et al.*, *Embo J* **20**, 2202 (May 1, 2001).
S7. J. Avery *et al.*, *J Cell Biol* **148**, 317 (Jan 24, 2000).
S8. K. I. Willig, S. O. Rizzoli, V. Westphal, R. Jahn, S. W. Hell, *Nature* **440**, 935 (Apr 13, 2006).
S9. G. Ficz, R. Heintzmann, D. J. Arndt-Jovin, *Development* **132**, 3963 (Sep, 2005).
S10. G. Ficz, *Göttingen, Univ., Diss.* (2005).
S11. D. Ermak, J.A. McCammon, *J. Chem. Phys.* **69**, 1352 (Aug, 1978).
S12. S. Takamori *et al.*, *Cell* **127**, 831 (Nov 17, 2006).
S13. S. W. Provencher, *Computer Physics Communications* **27**, 213 (1982).